Available online at www.sciencedirect.com

ScienceDirect

Journal of Magnesium and Alloys 2 (2014) 109−115
www.elsevier.com/journals/journal-of-magnesium-and-alloys/2213-9567

Full length article

Microstructures and mechanical properties of the age hardened Mg−4.2Y−2.5Nd−1Gd−0.6Zr (WE43) microalloyed with Zn

Y.H. Kang [a,b], D. Wu [a], R.S. Chen [a,*], E.H. Han [a]

[a] State Key Laboratory for Corrosion and Protection, Institute of Metal Research, Chinese Academy of Sciences, 62 Wencui Road, Shenyang 110016, China
[b] University of the Chinese Academy of Sciences, Beijing 100049, China

Received 13 November 2013; accepted 5 January 2014
Available online 18 June 2014

Abstract

The effect of trace addition of 0.2 wt.% Zn on the microstructures and mechanical properties of the age-hardening Mg−4.2Y−2.5Nd−1Gd−0.6Zr (wt.%) (WE43) alloy has been investigated. As compared with the WE43 alloy after solid solution treatment at 525 °C, the block-like Zn−Zr phase was still observed in the WE43-0.2Zn alloy. However, the time for WE43-0.2Zn alloy to get peak hardness at 250 °C was two hours, a half earlier than that in WE43 alloy, meaning a accelerated age precipitation kinetics has been achieved due to the addition of 0.2 wt.% Zn. Microalloyed with 0.2 wt.% Zn enhanced the ultimate tensile strength (UTS) slightly and ductility significantly both in the solutionized and peak aged condition. The enhancement in strength and ductility is possible associated with the larger volume fraction of precipitation phases due to a reduction of the solubility of rare earth elements (RE) in the α-Mg matrix, the larger aspect ratio (length to width) of precipitates and a decrease in stacking fault energy by addition of Zn.

Keywords: Magnesium alloy; Microalloying; Microstructures; Mechanical properties

1. Introduction

The strong need for weight reduction of transportation vehicles for better fuel efficiency has indicated magnesium alloys as a good potential structural material for many structural applications due to their high specific strength, high stiffness and good damping capacity combined with quite low density [1,2]. There has been a rapid growth in interest in the development of higher strength, creep-resistant Mg alloys for the automotive and aerospace industries [3,4]. The most successful Mg alloys developed to date have been those based on the Mg−Y−Nd system, identified as WE54 and WE43 [5−7]. The strength of these alloys is achieved essentially via precipitation strengthening [8]. The characteristics of the precipitates in Mg−Y−Nd alloys, such as crystal structure, morphology, size, precipitation sequence and phase evolution have been much investigated. Depending on the ageing temperature, the precipitation sequence in WE alloys has been reported to involve formation of phases designated β″, β′, β_1 and β, which all four precipitate phases have been described to form as plates on prismatic planes of the Mg matrix phase [5,6,9−13].

J.F.Nie has discussed the predicted strengthening effect of precipitates of different shape and habit on the basal and {10−12} twinning deformation systems in Mg by the development of the Orowan equation. It revealed that whether

* Corresponding author.
E-mail addresses: yhkang11s@imr.ac.cn (Y.H. Kang), dwu@imr.ac.cn (D. Wu), rschen@imr.ac.cn (R.S. Chen), ehhan@imr.ac.cn (E.H. Han).
Peer review under responsibility of National Engineering Research Center for Magnesium Alloys of China, Chongqing University

Production and hosting by Elsevier

http://dx.doi.org/10.1016/j.jma.2014.01.010.

particles are sheared or are shear resistant, and whether the deformation mode is basal slip or twinning, precipitate plates formed on prismatic planes of the Mg matrix phase provide the most effective barrier to gliding dislocations and propagating twins in the Mg matrix. It further suggest that a higher strength can be achieved if a high density of intrinsically strong, plate-shaped precipitates with prismatic and basal habit planes and of large aspect ratio can be developed in the microstructure by microalloying additions [8,14]. Zn is one of alloy elements with low cost and maximum solubility in solid Mg of 6.2 wt.%. The Mg alloys containing Zn possess excellent high mechanical properties [15]. Recently, a lot of work has been focused on Mg–RE alloys containing Zn elements, such as Mg–Y–Zn, Mg–Gd–Zn, Mg–Gd–Y–Zn alloys. It was reported that a certain amount of Zn added to Mg–Y, Mg–Gd and Mg–Y–Nd alloys improves the creep strength [16–20]. It also was reported that a certain amount of Zn added to Mg–Gd–Y alloys brought out the precipitations of long-period stacking ordered (LPSO) structures, which resulted in the decrease in volume fraction of the metastable phase in the aged condition [21]. However, Mg–Y–Nd alloys microalloyed with Zn have not been deeply investigated yet. In the present work, the effect of trace addition of 0.2 wt.% Zn on the microstructures and mechanical properties of the age-hardening WE43 alloy has been investigated.

2. Experimental procedures

Two Mg alloys with nominal compositions of Mg–4.2Y–2.5Nd–1Gd–0.6Zr (WE43) and Mg–4.2Y–2.5Nd–1Gd–0.2Zn–0.6Zr (WE43-0.2Zn) were prepared from high purity Mg (>99.95%), Y (>99%), Nd (99%), Gd (99%), Zn (99.9%) and a Mg–30Zr (wt.%) master alloy by melting in an electric resistance furnace at about 780 °C under protection with an anti-oxidizing flux. The melt was poured into a mild steel mold preheated to 200–300 °C. The detailed compositions of the obtained ingots were determined by inductively coupled plasma atomic emission spectroscopy (ICP-AES) and the results listed in Table 1. Specemens cut from the cast ingots were solution treated at 525 °C for 8 h, quenched into water and then subsequently aged at 250 °C for various periods of time.

Differential Thermal Analysis (DTA) has been performed on specimen of as-cast WE43 alloy, with a SETARAM-SETSYS Evolution 18 apparatus under protective pure argon atmosphere. Vickers hardness testing was performed using 500 g load and a holding time of 15 s. Not fewer than 10 measurements were taken in each alloy. The samples for tensile tests had a gauge length of 10 mm,width of 3.5 mm and thickness of 2.5 mm. Tensile tests were performed at roon temperature (RT) with an initial strain rate of 1.0×10^{-3} s^{-1}. At least three specimens were used for each condition to ensure the reproducibility of data and the average values were adopted.

Table 1
Analyzed chemical compositions of the investigated alloys (wt.%).

	Elements					
	Y	Nd	Gd	Zn	Zr	Mg
WE43	4.38	2.72	1.10	<0.01	0.56	Bal
WE43-0.2Zn	4.20	2.66	1.09	0.21	0.50	Bal

The constituent phases of the two alloys in different conditions were identified by X-ray diffraction (XRD) (Rigaku D/max 2500PC X-ray diffractometer) with Cu Kα radiation. Microstructures were observed by optical microscope (OM), scanning electron microscope (SEM, Philips XL30 ESEM-FEG/EDAX) and transmission electron microscope (TEM, JEM-2100F) operating at 200 kV. Samples in as-cast and ageing condition for optical microscopy were etched in a solution of 4 vol.% HNO_3 in ethanol after mechanical polishing. Samples in solution condition for optical microscopy were etched in a solution of 6 g picric acid, 40 ml acetic acid, 40 ml water and 100 ml ethanol. The mean grain size, d, was measured by the linear intercept method using the equation $d = 1.74L$, where L is the liner intercept grain size determined by optical microscopy. Compositions of phases were analyzed by energy dispersive X-ray spectrometry (EDS) in the SEM mode. Thin foil specimens for TEM were prepared by punching 3 mm diameter discs, followed by dimple grinding and Ar+ ion milling in a precision ion polishing system (PIPS, Gatan 691) operating at 4.5 kV accelerating voltage and ~8°incident angle.

3. Results

3.1. Characterization of the alloys in the as-cast state

Typical microstructures of WE43 alloy in the as-cast condition are shown in Fig. 1. It reveals that the as-cast of WE43 alloy consists mainly of the α-Mg phase (a solid solution of Mg containing Y, Nd and Gd) as the matrix and non-equilibrium eutectics which mainly aggregate at the grain boundaries, cuboid-shaped phase. Some zirconium cores are observable, which contribute to the grain refinement. The microstructure of the WE43-0.2Zn alloy is similar to that of the WE43 alloy. The average grain size of WE43 and WE43-0.2Zn alloy is about 94 μm and 106 μm, respectively. The composition of the eutectics (phase A) is Mg–6.41 at.% Nd–4.27 at.% Y–1.02 at.% Gd and the composition of the cuboid-shaped phase (phase B) is Mg–72.00 at.% Y–4.05 at.% Nd–5.07 at.% Gd, which are detected by EDS analyses in Fig. 1e and f. However, the composition of the eutectics is Mg–7.95 at.% Nd–4.83 at.% Y–1.18 at.% Gd–2.01 at.% Zn in the WE43-0.2Zn alloy, which is indicated that the microalloyed element Zn is partial dissolved in the eutectics. By XRD analysis (Fig. 2a), three phases are identified namely α-Mg, $Mg_{12}Nd$ and $Mg_{24}Y_5$.

3.2. Characterization of the solution-treated alloys

In order to determine its solution temperature, a preliminary DTA investigation (Fig. 2b) on a small quantity of

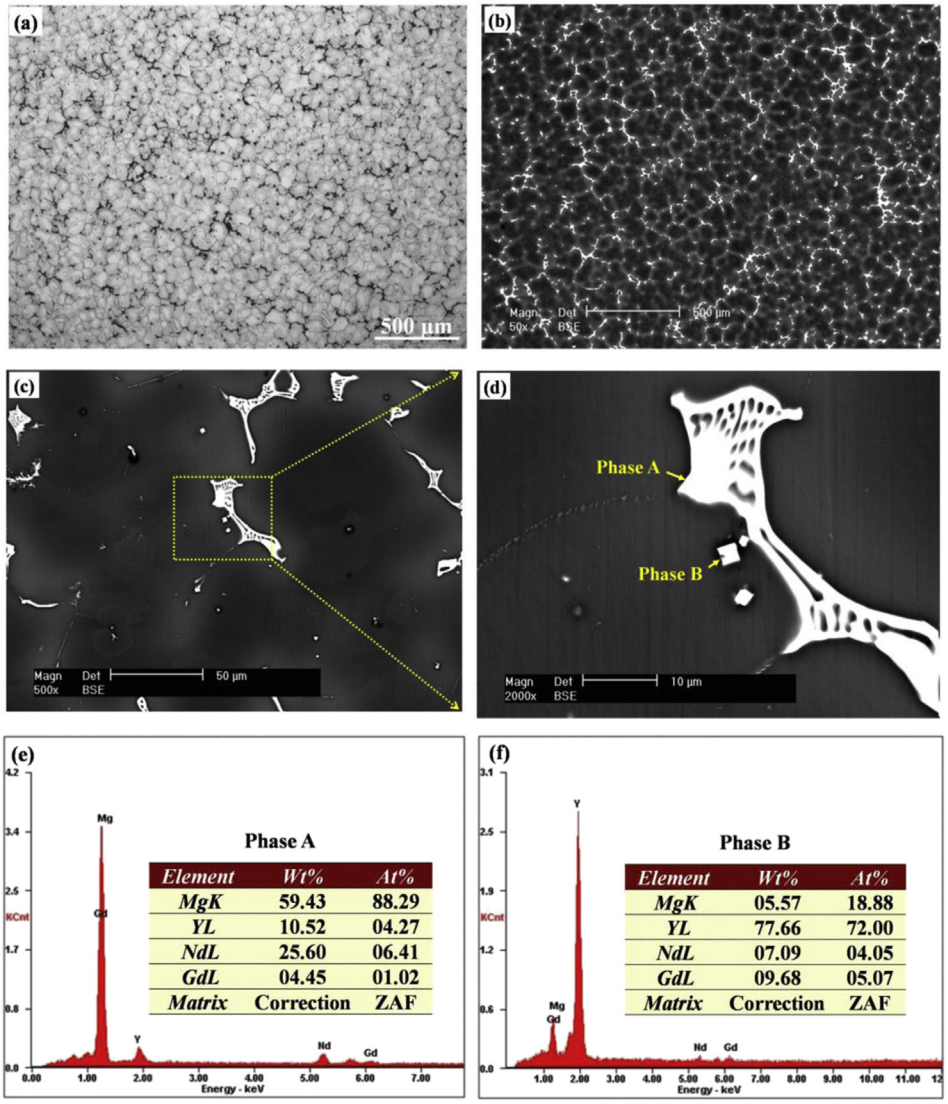

Fig. 1. Optical micrograph and SEM images obtained from the as-cast of WE43 alloy: (a) OM image; (b–d) SEM images; (e) the EDS result of the phase A; and (f) the EDS result of the phase B.

as-cast WE43 alloy was made. It can be obtained that the melting temperature of the eutectic phase is about 543 °C. So the temperature of 525 °C was chosen to dissolve the maximum quantity of solute atoms into the magnesium matrix and prevent over-heating. Fig. 3 shows the optical and SEM microstructures of the WE43 and WE43-0.2Zn alloys after the solution treatment at 525 °C for 8 h. Almost all the eutectics have dissolved into the matrix. XRD pattern

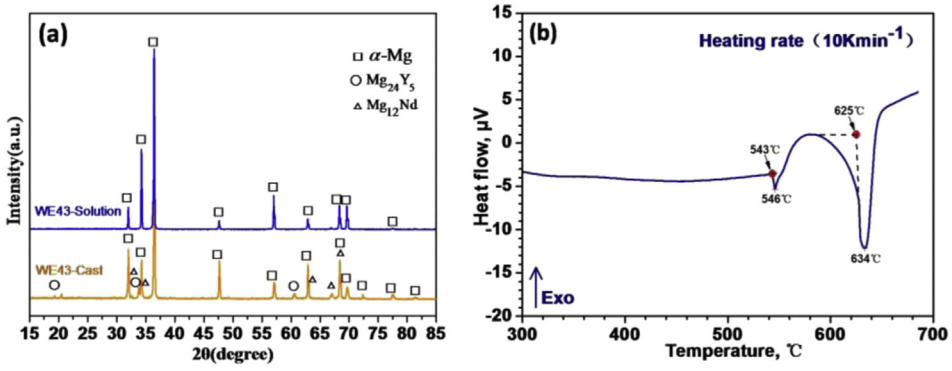

Fig. 2. (a) X-ray diffraction patterns of the WE43 alloy in the as-cast and solution-treated conditions; (b) DTA traces of as-cast WE43 sample up to melting. Heating rate is labeled.

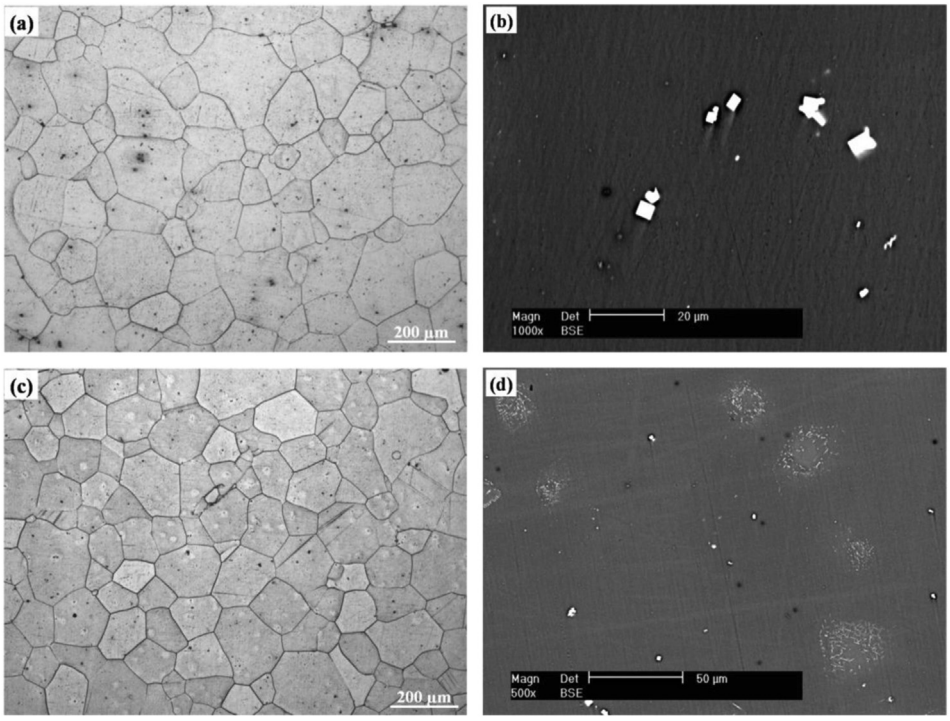

Fig. 3. Microstructures of the alloys in the solution-treated condition. (a)(c) Optical image showing the grain size and (b)(d) SEM image showing the cuboid-shaped phase and gathered clusters in WE43 and WE43-0.2Zn alloy, respectively.

(Fig. 2a) further confirms the dissolution of the eutectics. However, for both of the alloys, the cuboid-shaped phases are not dissolved, as shown in the high magnification of back-scattered electron micrograph (Fig. 3b and d). Moreover, some block-like compounds in gathered clusters can be observed in the solution-treated WE43-0.2Zn alloy (Figs. 3d and Fig.4), which contain elements of Zn and Zr. In addition, the average grain size of the WE43 and WE43-0.2Zn grows

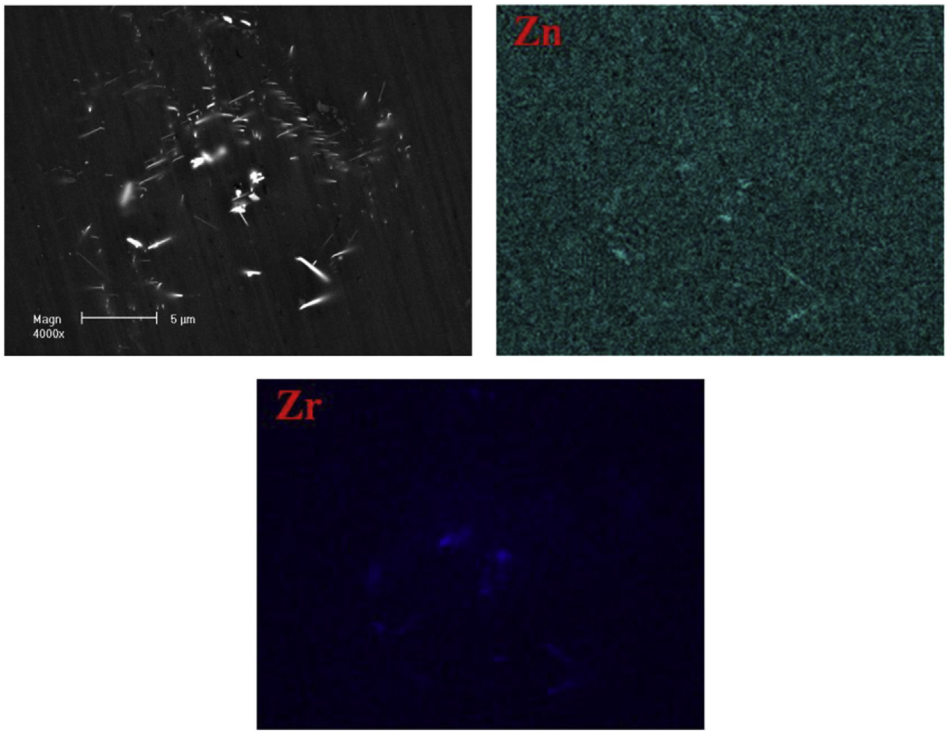

Fig. 4. The elements mapping for the gathered block-like phases in the solution-treated WE43-0.2Zn alloy.

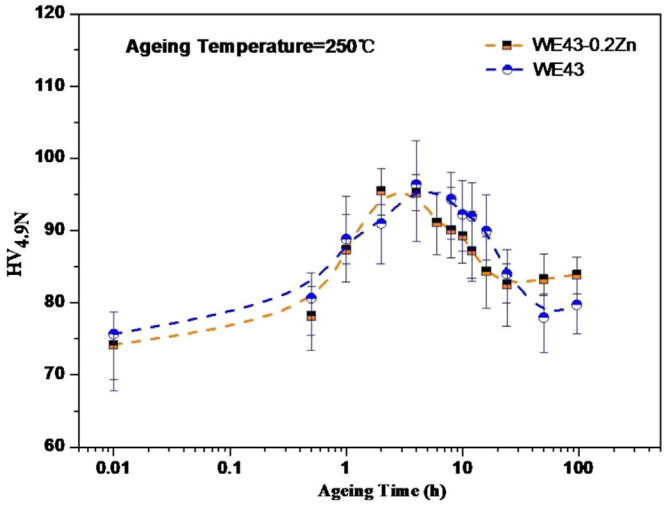

Fig. 5. Age-hardening curves of WE43 and WE43-0.2Zn alloys at 250 °C.

up to 184 μm and 146 μm after the solution treatment, respectively.

3.3. The age hardening behavior and mechanical properties

Fig. 5 compares the age hardening behaviors of WE43 and WE43-0.2Zn alloy with ageing at 250 °C. Initially, both of the alloys exhibit little age hardening responses until 0.5 h, and then the hardness increases rapidly. The peak hardness of WE43 is almost the same as that of WE43-0.2Zn alloy. However, the time for WE43-0.2Zn alloy to get peak hardness was two hours, a half earlier than that in WE43 alloy, when it was aged at 250 °C, meaning a accelerated age precipitation kinetics has been achieved due to the addition of 0.2 wt.% Zn. As the aging process continues, the hardness decreases rapidly up to a stability, but the stable hardness of the WE43-0.2Zn alloy is slightly higher.

The optical microstructure of aged samples is similar to that of solutionized one and the grain size does not change during ageing. Fig. 6a and b presents a TEM bright field $<0001>_{\alpha}$ micrograph of precipitates in a peak-aged sample of WE43 and WE43-0.2Zn alloy, respectively. It can be observed that the plate-shaped precipitates were in contact with irregular globular precipitates, which were commonly distributed in clusters. The globular precipitates were identified to be β′ phase and the plate-shaped precipitates were identified to be β1 or partly of β phase [9]. But as shown in Fig. 6, the sizes of precipitates is smaller and the aspect ratio (length to width) is larger by additions of 0.2 wt.% Zn to the WE43 alloy.

A comparison of the typical mechanical properties of the solution-treated and peak-aged WE43 and WE43-0.2Zn alloy is presented in Fig. 7 and Table 2. In solution-treated condition, microalloyed with 0.2 wt.% Zn enhanced the UTS slightly from 203.9 Mpa to 217.5 Mpa, but significantly enhanced the elongation from 6.87% to 13.2%. And also in peak-aged condition, microalloyed with 0.2 wt.% Zn enhanced the UTS slightly from 283.5 Mpa to 297.6 Mpa, but significantly enhanced the elongation from 2.35% to 4.6%. So additions of 0.2 wt.% Zn to the

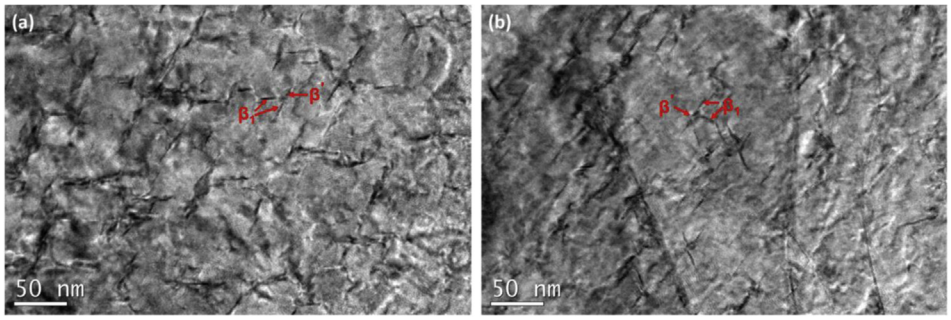

Fig. 6. The TEM bright field $<0001>_{\alpha}$ micrographs showing assemblies of plate-shaped and irregular globular precipitates in peak-aged samples at 250 °C of both (a) WE43 and (b) WE43-0.2Zn alloys.

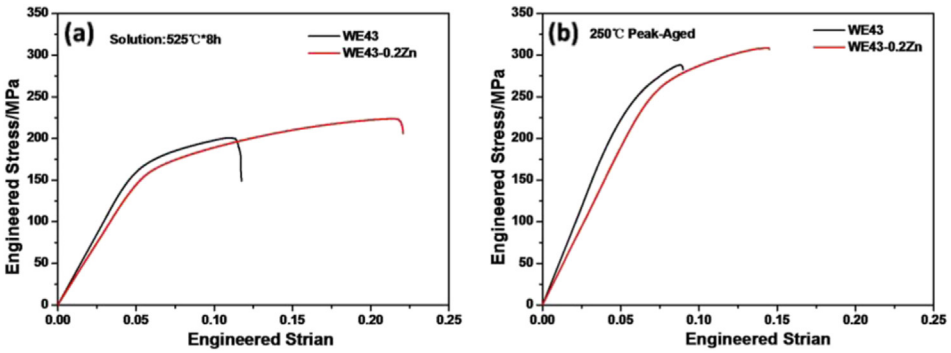

Fig. 7. Typical nominal stress–strain curves at room temperature for the WE43 and WE43-0.2Zn alloys in (a) solution-treated and (b) peak-aged at 250 °C.

Table 2
Tensile properties of the WE43 and WE43-0.2Zn alloys at room temperature.

Temper	Solution-treated		Peak-aged at 250 °C	
	WE43	WE43-0.2Zn	WE43	WE43-0.2Zn
Nominal UTS (Mpa)	203.9	217.5	283.5	297.6
Nominal TYS (Mpa)	144.5	140.6	221.9	240.1
Nominal elongation (%)	6.87	13.2	2.35	4.6

WE43 alloy lead to a slightly enhancement in ultimate tensile strength (UTS), but a considerable increase in ductility. This strengthening effect and increase in ductility will be discussed in the following section.

The Fig. 8 shows the typical secondary electron (SE) SEM images of the fracture surfaces of tensile specimens of WE43 and WE43-0.2Zn alloy in solution-treated and peak-aged conditions. The fracture surfaces of WE43 alloy in Fig. 8a and c are mainly composed of cleavage planes and tear ridges, but the proportion of cleavage plane and tear ridge is higher and smaller than WE43-0.2Zn alloy as shown in Fig. 8b and d, respectively, which is in accordance with a considerable increase in ductility by additions of 0.2 wt.% Zn. Especially, the fracture surface of solution treated WE43-0.2Zn alloy as shown in Fig. 8b is mainly composed of ductile transgranular cleavage planes of coarse dimples and tear ridges, which is in accordance with its high elongation of 15.2%.

4. Discussion

This study has shown microstructure evolutions relating to the mechanical properties, involving Vickers hardness and tensile stress–strain curves of WE43 and WE43-0.2Zn in solution-treated and peak-aged at 250 °C. The as-cast microstructure of the WE43-0.2Zn alloy detected by OM and SEM is the same as WE43 alloy, possibly due to the content of element Zn is too low to form new phases like long-period stacking ordered structures (LPSO) in Mg–Y–Zn alloys [22,23]. But in solution treated condition, as shown in Figs. 4 and 5, block-like Zn–Zr phases in gathered clusters can be observed in WE43-0.2Zn alloy, which is possible of the relative high content Zr to Zn in the center of grain leads to form Zn–Zr compounds during long time and high temperature solution treatment [24]. Obviously as presented in Fig. 7 and Table 2, higher ultimate tensile strength values and a considerable increase in ductility are obtained in WE43 alloy after adding 0.2 wt.% Zn. Suzuki et al. suggested that the strengthening effects of Zn might be due to decrease in stacking fault energy and consequent reduction of mobility of dislocations [18]. Besides, with the addition of 0.2 wt.% Zn to WE43, it will further decrease the RE solubility in magnesium, and there will occur larger volume fraction of precipitation phases. And as shown, the sizes of precipitates is smaller and the aspect ratio (length to width) is larger by additions of 0.2 wt.% Zn to the WE43 alloy. All mentioned above may contribute to the enhancement of ultimate tensile strength by microalloyed with Zn. And the significantly enhancement of ductility may due to the decrease in stacking fault energy.

5. Conclusions

In the present study, the effect of trace addition of 0.2 wt.% Zn on the microstructures and mechanical properties of the age-hardening WE43 alloy has been investigated. The following results are obtained:

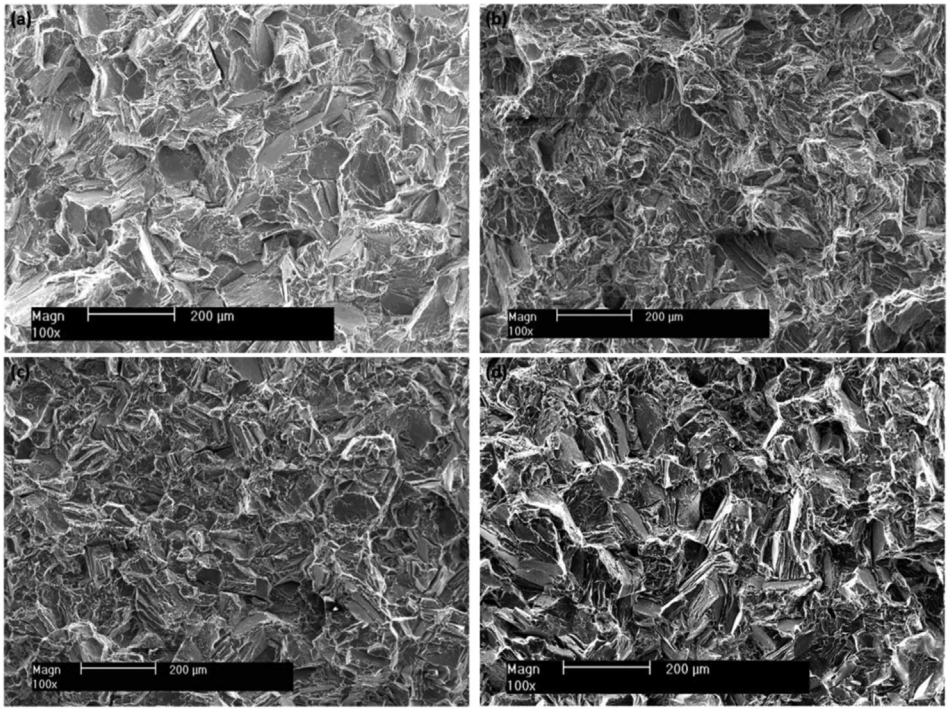

Fig. 8. Typical SEM images of fracture surfaces of tensile specimens tested at room temperature: (a) and (b) solution-treated; (c) and (d) peak-aged at 250 °C of WE43 and WE43-0.2Zn alloy, respectively.

1. The block-like Zn−Zr phase was observed in the WE43-0.2Zn after solid solution treatment at 525 °C, and the time for WE43-0.2Zn alloy to get peak hardness at 250 °C was two hours, a half earlier than that in WE43 alloy, meaning a accelerated age precipitation kinetics has been achieved due to the addition of 0.2 wt.% Zn.
2. Both in the solutionized and peak aged condition, additions of 0.2 wt.% Zn to WE43 alloy lead to a slightly enhancement in ultimate tensile strength (UTS), but a considerable increase in ductility.

Acknowledgments

This work was funded by the National Basic Research Program of China (973 Program) through project No. 2013CB632202.

References

[1] B. Mordike, T. Ebert, Mat. Sci. Eng. A 302 (2001) 37−45.
[2] A.A. Luo, J. Magnesium Alloy 1 (2013) 2−22.
[3] X. Li, W. Qi, K. Zheng, N. Zhou, J. Magnesium Alloy 1 (2013) 54−63.
[4] I.J. Polmear, Mater. Sci. Technol. 10 (1994) 1−16.
[5] H. Karimzadeh, Ph.D. Thesis, University of Manchester, U.K., 1985.
[6] G.W. Lorimer, C. Baker, G.W. Lorimer, W.Unsworth (Eds.), Proceedings of the London Conference on Magnesium Technology, The Institute of Metals, London, U.K, 1986, p. 47.
[7] P. Vostry, I. Stulikova, B. Smola, M. Cieslar, B.L. Mordike, Z. Metall. 79 (1988) 340−344.
[8] J.F. Nie, Metall. Mater. Trans. A 43 (2012) 3891−3939.
[9] J.F. Nie, B. Muddle, Scr. Mater. 40 (1999) 1089−1094.
[10] J.F. Nie, B. Muddle, Acta Mater. 48 (2000) 1691−1703.
[11] C. Antion, P. Donnadieu, F. Perrard, A. Deschamps, C. Tassin, A. Pisch, Acta Mater. 51 (2003) 5335−5348.
[12] C. Antion, P. Donnadieu, C. Tassin, A. Pisch, Philos. Mag. 86 (2006) 2797−2810.
[13] G. Barucca, R. Ferragut, F. Fiori, D. Lussana, P. Mengucci, F. Moia, G. Riontino, Acta Mater. 59 (2011) 4151−4158.
[14] J.F. Nie, Scr. Mater. 48 (2003) 1009−1015.
[15] E.F. Emley, Principles of Magnesium Technology, Pergamon Press, 1966.
[16] M. Suzuki, T. Kimura, J. Koike, K. Maruyama, Scr. Mater. 48 (2003) 997−1002.
[17] J.F. Nie, X. Gao, S. Zhu, Scr. Mater. 53 (2005) 1049−1053.
[18] M. Suzuki, T. Kimura, J. Koike, K. Maruyama, Mater. Sci. Eng. A 387 (2004) 706−709.
[19] J.F. Nie, K. Oh-Ishi, X. Gao, K. Hono, Acta Mater. 56 (2008) 6061−6076.
[20] J. Morgan, B. Mordike, Metall. Trans. A 12 (1981) 1581−1585.
[21] T. Honma, T. Ohkubo, S. Kamado, K. Hono, Acta Mater. 55 (2007) 4137−4150.
[22] X. Shao, Z. Yang, X. Ma, Acta Mater. 58 (2010) 4760−4771.
[23] Y. Zhu, A. Morton, J. Nie, Acta Mater. 58 (2010) 2936−2947.
[24] X. Gao, J.F. Nie, L.M. Peng, C.Q. Zhai, P.H. Fu, H.Y. Jiang, Mater. Sci. Forum 546 (2007) 97−100.